

This is an Open Access document downloaded from ORCA, Cardiff University's institutional repository:<https://orca.cardiff.ac.uk/id/eprint/112790/>

This is the author's version of a work that was submitted to / accepted for publication.

Citation for final published version:

Abbasi, Fayyaz-Ur-Rehman, Ali, Aamir, Alves, Tiago and Rehman, Khaista 2018. The accuracy of AVA approximations in isotropic media assessed via synthetic numerical experiments: Implications for the determination of porosity. *Journal of Petroleum Science and Engineering* 170 , pp. 563-575. 10.1016/j.petrol.2018.06.082

Publishers page: <https://doi.org/10.1016/j.petrol.2018.06.082>

Please note:

Changes made as a result of publishing processes such as copy-editing, formatting and page numbers may not be reflected in this version. For the definitive version of this publication, please refer to the published source. You are advised to consult the publisher's version if you wish to cite this paper.

This version is being made available in accordance with publisher policies. See <http://orca.cf.ac.uk/policies.html> for usage policies. Copyright and moral rights for publications made available in ORCA are retained by the copyright holders.





22

23

## Abstract

24 Analyses of seismic amplitude vs. angle are widely used to estimate hydrocarbon reservoir  
25 properties. In this paper we have investigated the accuracy of existing approximations based on  
26 the Zoeppritz equation, using synthetic numerical experiments that correlate P-wave reflectivity  
27 in isotropic media with reservoir porosity. An effective medium non-interacting approach (NIA)  
28 in rock physics modelling was used to compute the properties of fluid-saturated (water + gas)  
29 reservoir, which were then used in seismic modelling. In parallel, a Bayesian approach was used  
30 to estimate reservoir porosities from angle-dependent reflection coefficients and seismic  
31 amplitudes. A *Maximum a posteriori* solution of the Bayesian approach was also utilised to obtain  
32 an inverted porosity distribution in the reservoir model. The results of our forward models are  
33 important as they suggest that most of the approximations deviate from the exact Zoeppritz  
34 solutions with increasing angles of incidence of seismic waves. The results from the Bayesian  
35 inversion show that the Rüger and Bortfeld approximations agree with the exact Zoeppritz  
36 solutions to accurately estimate reservoir porosity. All the other approximations, except for  
37 Smith's, underestimate reservoir porosity and should be used in pre-stack inversion with caution.  
38 Smith's and Fatti's approximations failed to estimate reservoir porosity because of associated  
39 uncertainties.

40

41 **Keywords:** Seismic amplitude vs. angle; Rock physics modelling, Non-interacting approach,  
42 Bayesian approach, Metropolis algorithm, Pre-stack seismic inversion.

43

44

## 45 **1. Introduction**

46 The analysis of seismic amplitude variation with angle of incidence (AVA) is commonly used in  
47 the evaluation of porosity, lithology and fluids in hydrocarbon reservoirs. This analysis can  
48 become further useful when integrated with appropriate rock physics models. The roots of AVA  
49 analyses derive from the classical writings of Green (1839) and Knott (1899), who have studied  
50 the effect of interfaces on the reflection and transmission of seismic waves. In addition, Zoeppritz  
51 (1919) published a series of equations, among which the most important is the Zoeppritz equation  
52 regarding the partition of energy across isotropic media. This equation expressed the partition of  
53 energy of a plane wave when it hits the interface between two isotropic layers with different  
54 properties. As a result, several approximations to the exact Zoeppritz solution have been used in  
55 AVA analyses of isotropic media around the globe due to their relative ease of applicability  
56 (Bortfeld 1961; Aki and Richards 1980; Shuey 1985; Smith and Gidlow 1987; Hilterman 1989;  
57 Fatti et al. 1994; Rüger 2002).

58 The validity of the approximations described above depends on key assumptions used in their  
59 formulation. Each approximation describes the P-wave reflection coefficient as a function of a  
60 wave's angle of incidence and local rock properties such as the compressional and shear wave  
61 velocities, density, Poisson's ratio and other elastic parameters. These approximations are widely  
62 used because they are empirical and able to explain the AVA phenomenon on seismic, to then  
63 return meaningful physical properties of sub-surface units. For instance, the Shuey's  
64 approximation (Shuey 1985) tells us about the intercept (reflection strength at zero offset), gradient  
65 (the rate of change of reflection strength with incident angle) and curvature (the rate of change of  
66 reflectivity gradient) of a seismic wave. These AVA attributes are particularly helpful in the  
67 identification of low impedance gas sands (Castagna and Swan 1997).

68 Rock Physics Modelling acts as a bridge between seismic and rock properties, having a crucial  
69 role in seismic reservoir characterization (Avseth et al. 2005). Rock Physics Modelling plays a  
70 significant role in linking elastic parameters, such as impedance and velocity, to reservoir  
71 properties of interest (lithology, porosity and pore fluids; Wang 2001; Bosch et al. 2010). Rock  
72 Physics Modelling is widely combined with geostatistical techniques in seismic inversion.  
73 Combining rock physics data with geo-statistics during seismic inversion can be helpful to reduce  
74 uncertainties (Mukerji et al. 2001). By comparing this modelled (calculated) seismic data with raw  
75 (observed) seismic data, desired rock parameters can be calculated by iteratively using stochastic  
76 approaches (Grossman, 2003; Shahraini et al. 2011; Ali and Jakobsen 2011a; Ali and Jakobsen  
77 2011b; Ali and Jakobsen 2014; Ali et al. 2015).

78 Pre-stack seismic inversion is widely used to estimate reservoir properties in the petroleum  
79 industry. This is a complicated process because it is an ill-posed problem with a non-unique  
80 solution. Therefore, it is important to overcome these challenges in order to estimate reservoir  
81 properties up to a satisfactory level. In order to overcome the problem of model instability, Du and  
82 Yan (2013) proposed a method for the estimation of fluid factors by utilising offset-limited data.  
83 Liang et al., (2017) addressed the same problem by utilising edge-preserving regularization and a  
84 Markov random field. Chiappa and Mazzotti (2009) formulated a linear Bayesian inversion  
85 method to estimate petrophysical properties. Sun et al. (2015) introduced pre-stack elastic  
86 integration techniques by considering the impact of rock physics and amplitude-preserving  
87 processing algorithms on pre-stack inversion. Finally, Anwer et al. (2017) utilised an anisotropic  
88 T-matrix approach in a Bayesian inversion scheme to characterise anisotropic sand-shale medium.  
89 The aim of this study is to investigate the accuracy of existing approaches used in AVA modelling  
90 to determine porosity in isotropic media. In order to accomplish our aim, we have followed the

91 workflow presented in Figure 1. A rock physics model based on an effective medium approach  
92 was used to compute the effective properties for fluid saturated isotropic reservoir rocks. These  
93 properties were then utilised to compute P- and S-wave velocities ( $V_P$  and  $V_S$  respectively) and  
94 density ( $\rho$ ), and these two latter parameters were applied in a forward model to compute angle  
95 dependent P-wave reflection coefficients using the exact Zoeppritz solution, or approximations to  
96 the exact solution. AVA synthetic gathers were computed by convolving these reflection  
97 coefficients with a source wavelet. The exact Zoeppritz solution or approximations to the exact  
98 solution were used to invert the data to estimate porosity using a Bayesian approach and the  
99 Metropolis Algorithm of the Monte Carlo method (Tarantola 2005). Porosity distribution  
100 throughout the reservoir was also estimated using the *maximum a posteriori* solution of the  
101 Bayesian approach for each approximation, so we could investigate any implications of our  
102 methods to the determination of reservoir porosity.

103

## 104 **2. Forward Modelling**

105

106 The forward model used in this study can be written as:

$$\mathbf{d} = \mathbf{G}(\mathbf{m}). \quad (1)$$

107 Here  $\mathbf{d}$  is the vector of observed seismic AVA data,  $\mathbf{m}$  is a vector of unknown parameters (porosity  
108 in our case) and  $\mathbf{G}$  is a forward modelling operator, which is a combination of rock physics  
109 modelling and seismic attribute generation (AVA data). In the following section we present a brief  
110 description of rock physics and seismic modelling.

111

## 112 **2.1 Rock Physics Modelling**

113 The main purpose of rock physics is to understand the influence of rock properties, e.g. lithology,  
114 porosity, saturation, etc., on seismic velocities. There are several theories to estimate the elastic  
115 properties of dry and saturated rocks containing pores and cracks of different aspect ratios. Ali et  
116 al. (2015) showed a comparison between rock physics models based on effective stiffness and  
117 compliance methods for fractured reservoir characterization. A good rock physics model can  
118 efficiently estimate reservoir properties, which can then be correlated with seismic data to allow  
119 the modelling of an entire reservoir. Hence, a realistic model was assumed in this study containing  
120 a quartz matrix, interconnected spherical pores, randomly oriented micro-cracks that do not  
121 contribute to porosity, and a mixture of water and gas as pore saturating fluids (Figure 2). The  
122 input to rock physics model, in the form of elastic properties of quartz matrix and fluid, is given  
123 in Table 1.

124 We used a non-interacting approach (NIA) based on effective medium modelling to compute  
125 effective properties of isotropic reservoirs. Hudson and Knopoff (1989) proposed a relationship to  
126 obtain effective compliance  $\mathbf{S}^*$  for an isotropic medium, based on a NIA, as follows:

$$\mathbf{S}^* = \mathbf{S}^{(0)} - \sum_{r=1}^N (v^{(r)} (\mathbf{S}^{(0)} : \mathbf{C}^{(r)} - \mathbf{I}_4) : \mathbf{K}^{(r)}), \quad (2)$$

127 in which  $\mathbf{S}^{(0)}$  represents the compliance tensor of background matrix,  $v^{(r)}$  is the volume  
128 concentration of pores and randomly oriented micro-cracks, the stiffness tensor  $\mathbf{C}^{(r)}$  is associated  
129 with the inclusions (pores and randomly oriented micro-cracks),  $\mathbf{I}_4$  is the identity for fourth-rank  
130 tensors, and  $\mathbf{K}^{(r)}$  represents the K-tensor of Eshelby (1957) which can be given as (Jakobsen and  
131 Johansen 2005):

$$\mathbf{K}^{(r)} = \mathbf{A}^{(r)} : \mathbf{S}^{(0)}, \quad (3)$$

132 where,

$$\mathbf{A}^{(r)} = [\mathbf{I}_4 - \mathbf{G}^{(r)} : (\mathbf{C}^{(r)} - \mathbf{C}^{(0)})]^{-1}. \quad (4)$$

133 Here  $\mathbf{G}^{(r)}$  is a fourth-rank tensor given by the Green's function integrated over a characteristic  
 134 spheroid with the same shape as inclusions (pores and randomly oriented micro-cracks) of type  $r$   
 135 (Jakobsen et al. 2003; Ali and Jakobsen 2011a; Ali and Jakobsen 2011b; Ali and Jakobsen 2014).  
 136 In order to incorporate the case of empty inclusions, the stiffness parameter is taken out of the  
 137 equation so that Equation (2), for a dry rock, can be rewritten as (Hu and McMechan 2009):

$$\mathbf{S}^* = \mathbf{S}^{(0)} + \sum_{r=1}^N v^{(r)} \mathbf{K}^{(r)} \quad (5)$$

138 For the effect of fluid saturation we used the isotropic Gassmann's equation (Gassmann 1951),  
 139 which is given by:

$$K_{sat} = K_{dry} + \left( \frac{\left( 1 - \left( \frac{K_{dry}}{K_{frame}} \right) \right)^2}{\left( \frac{\varphi}{K_f} \right) + \left( \frac{1 - \varphi}{K_{frame}} \right) - \left( \frac{K_{dry}}{(K_{frame})^2} \right)} \right). \quad (6)$$

140 In Equation (6)  $K_{sat}$ ,  $K_{dry}$ ,  $K_{frame}$  and  $K_f$  represent the bulk modulus of fluid-saturated rock, dry  
 141 rock, dry rock frame and pore-saturating fluid, respectively, and  $\varphi$  represents porosity.  $K_f$  is  
 142 computed using Wood's relationship (Wood 1955), which is given by:

$$\frac{1}{K_f} = \frac{S_g}{K_g} + \frac{S_o}{K_o} + \frac{S_w}{K_w}. \quad (7)$$

143 In Equation (7),  $S_g$  and  $K_g$ ,  $S_o$  and  $K_o$ ,  $S_w$  and  $K_w$  are the saturation and bulk modulus of gas, oil  
144 and pore saturating water, respectively.

145 The effective moduli and density from this rock physics model were estimated for different  
146 porosities, and then used to compute P- and S-wave velocities. As the Lamé's parameter ( $\lambda$ ) and  
147 shear modulus ( $\mu$ ) are sufficient to characterise an isotropic medium, these moduli can also be  
148 expressed in terms of the stiffness parameters C11 and C44. The effect of porosity on P- and S-  
149 wave velocities, and stiffness parameters (C11 and C44), is shown in Figure 3. An increase in  
150 porosity weakens a volume of rock by decreasing the bulk and shear moduli. As a result of this  
151 reduction, P- and S-wave velocities, together with the stiffness parameters above, decrease with  
152 increasing porosity. Such trends are more or less expected, but they would have been difficult to  
153 quantify without a suitable rock physics model.

154

## 155 **2.2 Seismic Modelling**

156 The solution of seismic forward modelling started with the development of numerical solutions  
157 for the wave equation (Krebes 2004). Two-dimensional (2D) seismic forward modelling can be  
158 undertaken using ray tracing, matrix method, finite difference and finite-element methods. One of  
159 the key parts in seismic forward modelling is the computation of reflection coefficients by utilising  
160 P- and S-wave velocities and density in the exact Zoeppritz solution, or approximations to the  
161 exact solution, as previously discussed. When an incident P-wave strikes an interface between two  
162 layers of different properties, at a non-zero incident angle, it is converted into four rays as shown

163 in Figure 4. The energy partition at the interface can be calculated using the Zoeppritz energy  
 164 equation re-written as follows (Pujol 2003):

$$165 \begin{bmatrix} R_{PP} \\ R_{PS} \\ T_{PP} \\ T_{PS} \end{bmatrix} = \begin{bmatrix} -\sin e & \cos f & \sin e' & \cos f' \\ \cos e & \sin f & \cos e' & -\sin f' \\ \sin 2e & -\left(\frac{v_p}{v_s}\right) \cos 2f & \left(\frac{\rho'}{\rho}\right) \left(\frac{v_p}{v_p'}\right) \left(\left(\frac{v_s'}{v_s}\right)^2\right) \sin 2e' & \left(\frac{\rho'}{\rho}\right) \left(\frac{v_p}{v_s'}\right) \left(\left(\frac{v_s'}{v_s}\right)^2\right) \cos 2f' \\ -\cos 2f & -\left(\frac{v_s}{v_p}\right) \sin 2f & \left(\frac{\rho'}{\rho}\right) \left(\frac{v_p'}{v_p}\right) \cos 2f' & \left(\frac{\rho'}{\rho}\right) \left(\frac{v_s'}{v_p}\right) \sin 2f' \end{bmatrix}^{-1} \begin{bmatrix} \sin e \\ \cos e \\ \sin 2e \\ \cos 2f \end{bmatrix}. \quad (8)$$

166 with:

167  $R_{PP}$  - P-wave reflection coefficient

168  $R_{PS}$  - S-wave reflection coefficient

169  $T_{PP}$  - P-wave transmission coefficient

170  $T_{PS}$  - S-wave transmission coefficients.

171 In Equation (8),  $v_p$ ,  $v_s$  and  $\rho$  are the P- and S-wave velocities and density of upper medium,  
 172 respectively.  $v_p'$ ,  $v_s'$  and  $\rho'$  are P- and, S-wave velocities and density of the gas reservoir  
 173 respectively. In addition,  $e$  and  $e'$ , and  $f$  and  $f'$  are the reflection and transmission angles of P-and  
 174 converted S-wave respectively.

175 From the original Zoeppritz equations, different seismic amplitude vs. offset (AVO)  
 176 approximations can be classified into linear and nonlinear AVO approximations (Rüger 2002).

177 The key assumptions leading to linear AVO approximations are justified by the fact that certain  
 178 sedimentary rocks show weak to moderate contrasts in elastic parameters (Thomsen 1986;  
 179 Thomsen 1995). The exact Zoeppritz solution and approximations to exact solution are dependent  
 180 upon the angle of incidence, at which the seismic wave strikes an interface, but generally the  
 181 seismic data is a function of offset. This same offset should be converted in an angle during the  
 182 application of processing algorithms. This type of analysis is called as AVA instead of AVO.

183 In order to perform AVA modelling, P and S-wave velocities and density obtained from rock  
184 physics modelling are placed in Equation (8), or approximations to Equation (8), to compute  
185 reflection coefficients for different angles of incidence of a seismic wave. These angle dependent  
186 reflectivities can be convolved with source wavelet to obtain an AVA seismic response.

187 In this study, a rock physics model was iteratively used to compute effective moduli and density  
188 for different porosities at reservoir level. The sensitivity of P-wave reflection coefficient for  
189 porosity, using the exact Zoeppritz solution and approximations to the exact solution, is shown in  
190 Figure 5. The values of P-wave reflection coefficient are greater for smaller porosity and decrease  
191 with increase in porosity. In turn, velocity and density of the medium are responsible for this  
192 behaviour because they increase with decreasing porosity, and vice-versa. P-wave reflection  
193 coefficient for the exact Zoeppritz solution along with its approximations decreases with a relative  
194 increase in the angle of incidence, and form Class-1 AVO anomalies according to Rutherford and  
195 Williams (1989).

196

### 197 **3. Inverse modelling**

198 Seismic inversion is an important tool to estimate rock properties from seismic data using a  
199 combination of rock physics and statistical techniques. There are different approaches for the  
200 quantitative estimation of reservoir properties using seismic inversion. The scientific study of a  
201 physical system can be conducted in three steps: a) parameterisation of the system, b) forward  
202 modelling, and c) inverse modelling (Tarantola 2005). A non-linear inverse problem is considered  
203 in this study as:

$$G(m) \approx d. \quad (9)$$

204 Here  $\mathbf{m}$  represents a vector of physical parameters related to the porosity of the Earth model, and  
205  $\mathbf{d}$  is data vector of observed values, i.e. in this work, the angle dependent reflectivity/seismic AVA  
206 gathers.  $\mathbf{G}$  is a combination of the rock physics and seismic attributes, i.e. angle-dependent  
207 reflectivity/seismic gathers as a function of porosity.

208 A real physical system is best modelled by incorporating the effect of noise in forward model.  
209 Therefore, by including the noise term in Equation (9) (Aster et al. 2005), we have:

$$\mathbf{G}(\mathbf{m}) \approx \mathbf{d} + \eta. \quad (10)$$

210 In Equation (10),  $\eta$  represents the noise vector and generally it is assumed to be Gaussian  
211 (Tarantola 2005; Aster et al. 2005). The noise in seismic data is mainly introduced during its  
212 acquisition, and can be coherent (originated due to seismic source) or incoherent (noise introduced  
213 due to some other sources like traffic, wind, river, high tension wires above geophones etc.).  
214 Incoherent noise is also called random noise because its behaviour varies for each shot gather in a  
215 data volume. This noise can be minimised by increasing the fold of seismic data. Coherent noise  
216 includes diffractions, refractions, multiples, etc., and should be removed by the application of  
217 sophisticated processing algorithms before performing AVA inversion (Grossman 2003; Zhang et  
218 al. 2014; Marfurt and Alves 2015).

219 We used a Bayesian approach to get the probability distribution of porosities from our forward  
220 modelling. The Bayes' theorem (Aster et al. 2005) provides a framework in which the posterior  
221 probability of the variables of interest, derived from uncertain data, is obtained using *a priori*  
222 information. This *a priori* information is used to obtain unique maxima of Probability Density  
223 Functions (PDF) and makes solutions stable when using uncertain data (Duijndam 1988a, 1988b).  
224 The probabilistic prediction provides a natural way of understanding the uncertainty of the

225 problem. Uncertainties in a Bayesian framework for AVO inversion were discussed by Houck  
226 (2002).

227 An inverse problem is solved using a Bayesian approach that combines the prior distribution  $P(\mathbf{m})$   
228 for the model parameters with the likelihood function  $P(\mathbf{d}|\mathbf{m})$ . This way, one can obtain a  
229 posterior probability distribution  $P(\mathbf{m}|\mathbf{d})$  over a model space such as (Aster et al. 2005):

$$P(\mathbf{m}|\mathbf{d}) = \frac{P(\mathbf{m})P(\mathbf{d}|\mathbf{m})}{P(\mathbf{d})}. \quad (11)$$

230 In this equation, the posterior probability distribution  $P(\mathbf{m}|\mathbf{d})$  represents the solution of the inverse  
231 problem, and  $P(\mathbf{d})$  is considered as normalisation constant. The solution for a posterior probability  
232 density function (Aster et al. 2005) using a Gaussian approach is given by:

$$P(\mathbf{m}|\mathbf{d}) = N \cdot e^{-J(\mathbf{m})}. \quad (12)$$

233 In Equation (12), the constant N is called the normalization constant, and  $J(\mathbf{m})$  represents the  
234 objective function to be minimised. The objective function by assuming Gaussian statistics can be  
235 given as (Aster et al. 2005):

$$J(\mathbf{m}) = \frac{1}{2} [(\mathbf{G}(\mathbf{m}) - \mathbf{d})^T \mathbf{C}_D^{-1} (\mathbf{G}(\mathbf{m}) - \mathbf{d}) + (\mathbf{m} - \mathbf{m}_0)^T \mathbf{C}_M^{-1} (\mathbf{m} - \mathbf{m}_0)]. \quad (13)$$

236 Here,  $\mathbf{m}_0$  represents the mean value of the *a priori* distribution,  $\mathbf{C}_D$  is the covariance matrix for  
237 the data, and  $\mathbf{C}_M$  is the covariance matrix representing the model space. In case of uninformative  
238 prior information, Equation (13) can be represented by the likelihood function. The posterior  
239 distribution represents the full solution to an inverse problem. The evaluation of posterior  
240 distribution depends on the number of unknown parameters. As, in this study, we have only one  
241 unknown parameter (porosity), the posterior distribution given by Equations 12-13 represents the

242 solution of the inverse problem. In case of higher number of unknown parameters, the exploration  
243 of posterior distribution can be performed using the methods presented by Ali and Jakobsen  
244 (2011a), Ali and Jakobsen (2011b), Shahraini et al. (2011) and Ali and Jakobsen (2015).

245 We also used the Metropolis algorithm of the Monte Carlo method to estimate reservoir porosity  
246 using the exact Zoeppritz solution, and approximations to the exact solution. This method was  
247 developed by Metropolis and Ulam (1949), Metropolis et al. (1953) and Hastings (1970),  
248 consisting of a Markov Chain Monte Carlo (MCMC) technique used to estimate a solution by  
249 sampling through a posterior (arbitrary) distribution. The basic idea of this method is to sample  
250 the target distribution by performing a random walk, from sample to sample, and modify the walk  
251 according to some pre-defined conditions (Tarantola 2005).

252

## 253 **4 Results and Discussion**

254

### 255 **4.1. Accuracy in forward modelling**

256 Rock Physics Modelling was used to compute the effective moduli and density of a model  
257 presented in Figure 2. The aspect ratio of randomly oriented micro-cracks used in Rock Physics  
258 Modelling was set to 1/1000. The properties of the quartz matrix and fluids (water + gas) are given  
259 in Table 1.

260 The seismic velocity for the model was computed from these moduli, and from density, by iterating  
261 the rock physics model for different porosities discussed in section 2.1. These velocities and  
262 density were utilised in Equation (8), and approximations to Equation (8), in order to obtain angle-  
263 dependent P-wave reflectivity for different porosity values discussed in section 2.2. The properties

264 of overburden strata required to compute reflection coefficients are shown in Table 1. The  
265 comparison of the exact Zoeppritz solution (and approximations to the exact solution) for different  
266 porosities, with respect to the angle of incidence of seismic waves, is shown in Figure 6.

267 In Figure 6 one can observe that almost all the approximations, except Fatti and Smith's, are in  
268 good agreement with the exact Zoeppritz's solution at relatively small incidence angles. However,  
269 they start to deviate from the Zoeppritz's solution as the angle of incidence increases (Figure 6).  
270 The Fatti's approximation (Fatti et al. 1994) has a comparatively higher gradient and deviates from  
271 the exact Zoeppritz solution even at near-incidence angles. Importantly, Smith's reflectivity values  
272 (Smith and Gidlow 1987) start to increase and move away from the exact Zoeppritz solution with  
273 increasing porosity (Figure 6). All other approximations do not change their behaviour  
274 significantly with increasing porosity values (Figure 6).

275 The P-wave reflection coefficients obtained from a combination of rock physics and seismic  
276 modelling were convolved with source wavelet to obtain synthetic seismic AVA gathers for  
277 different porosity levels. These P-wave reflection coefficients are displayed in Figure 7 to 10 for  
278 porosity values of 0.1, 0.2, 0.3 and 0.4, respectively. All the approximations reveal a polarity  
279 reversal, with the Fatti's approximation having the largest negative amplitude - hence disagreeing  
280 with the exact Zoeppritz solution (Figures 7-10). The amplitude of synthetic AVA gathers shows  
281 a decreasing trend with respect to angle of incidence (Figures 7-10). Synthetic amplitude is higher  
282 at low porosities for all approximations, and decreases with increasing porosity.

283

#### 284 **4.2 Accuracy in inverse modelling**

285 In order to check the accuracy of P-wave reflection coefficient approximations for AVO  
286 inversions, we tried to retrieve true reservoir porosity (0.15) from synthetic reflection coefficient  
287 and amplitude data (with 25% noise/uncertainty/standard deviation of observed seismic data) using  
288 the Bayesian approach and the Monte Carlo method discussed in Section 3. Normally, the  
289 uncertainty (standard deviation/noise level) in seismic AVA data is within the range of 10-30%  
290 (Ren et al. 2017). Noise represents the uncertainty left in the observed data after the application of  
291 sophisticated seismic AVA-processing algorithms such as amplitude preserving migration  
292 (Grossman 2003; Zhang et al. 2014). The amplitude of seismic data is the most important factor  
293 in seismic AVA analyses, and preserving the true amplitude via sophisticated algorithms is crucial.  
294 We have considered an uninformative prior in our inverse problem, so the objective function is  
295 only represented by the likelihood function. The choice of uninformative prior gives an equal  
296 likelihood for all unknown parameters to be estimated during the inversion process. The source of  
297 prior information comes from independent measurements (e.g. well logs and laboratory  
298 measurements of porosity). The results of this inversion are shown in Figure 11 to 14. Figures 11-  
299 12 represent the inversion result in the form of a posterior distribution, whereas Figures 13-14  
300 represent the inversion result obtained via the sampling of the posterior distribution, i.e. a Monte  
301 Carlo method.

302 Rüger and Bortfeld's (Bortfeld 1961; Rüger 2002) approximations show a good agreement with  
303 the exact Zoeppritz solution, and associated uncertainties are comparatively smaller. Aki and  
304 Richards, Hilterman and Shuey's approximation (Aki and Richards 1980; Hilterman 1989; Shuey  
305 1985) underestimates reservoir porosity. In addition, the uncertainty for Smith's approximation is  
306 quite high and cannot be used in AVA inversion for reservoir porosity. It is also interesting to note  
307 that the inversion results from angle-dependent reflection coefficients and seismic amplitudes are

308 the same (Figures 11-12). This stems out from the fact that seismic amplitudes are basically the  
309 result of convolving reflection coefficients with a source wavelet.

310 Finally the *Maximum a posteriori* solution of the Bayesian approach was used to recover the  
311 porosity distribution in the reservoir. Initially, a Gaussian random porosity field (a smoothly  
312 varying field; Buland and Omre 2003) representing reservoir porosity was generated (100×100  
313 grid blocks), and this field was then compared with the porosity fields recovered by the exact  
314 Zoeppritz solution, and approximations to the exact solution, by minimising the objective function  
315 as:

$$316 \quad J(\mathbf{m}) = \sum_{i=1}^{40} \left[ \frac{R_i^C(\mathbf{m}) - R_i^O}{\Delta R_i} \right]^2. \quad (14)$$

317 In this equation,  $R_i^C$  and  $R_i^O$  are respectively the calculated and observed reflectivities. The term  
318 ‘ $\Delta R_i$ ’ in the denominator  $\Delta R_i$  represents the standard deviation (noise/uncertainty) present in the  
319 synthetic AVA data.

320 Results obtained from this latter procedure are shown in Figure 15. Porosities recovered by Rüger  
321 and Bortfeld’s approximations are in good agreement with the exact Zoeppritz solution, and  
322 recover reservoir porosities to a satisfactory level. In comparison, Aki and Richards, Hilterman  
323 and Shuey’s approximations underestimate porosity, with its effect being more prominent for  
324 smaller porosities. Fatti and Smith’s approximations completely failed to recover reservoir  
325 porosity due to their high associated uncertainty. Uncertainty associated with each approximation  
326 is shown in Table 2.

327 It is important to mention that the inversion results in Figures 11 to 14 represent the results in the  
328 form of a single grid block. The inverse numerical experiment presented in Figure 15, in the form  
329 of Gaussian field on 100×100 grid blocks for porosity, is very important in the context of its

330 application on raw data. More specifically, the inversion procedure presented in Figures 11 to 14  
331 is repeated for 100×100 grid blocks and the optimum (true) value of porosity is recovered utilising  
332 the *Maximum a posteriori* solution of the Bayesian approach. One can visually inspect the  
333 performance of approximations to the exact solution by comparing them with the result of exact  
334 Zoeppritz solution. This approach is, in this work, suggested as the most practical way of  
335 estimating the distribution of porosity in reservoir intervals using raw seismic data.

336

### 337 **4.3 Applications on raw seismic data**

338 For applications on raw seismic data, pre-stack seismic data processed typically for AVA/AVO  
339 analyses using the workflows given by Ostrander (1984), Chiburis (1984), Castagna and Backus,  
340 1993, Grossman (2003) and Zhang et al. (2014), are required along with well-log and any ancillary  
341 laboratory information. The petrophysical analysis of well-log data and laboratory measurements  
342 will provide the basic input parameters required to perform the Rock Physics Modelling necessary  
343 to obtain the effective elastic properties of the gas sand reservoir. Using these effective elastic  
344 properties, seismic modelling can be performed by exact Zoeppritz solution, or approximations to  
345 the exact solution (calculated data). From pre-stack seismic data (near, mid and far angle gathers),  
346 the amplitudes/angle-dependent reflection coefficients can be obtained at reservoir level (observed  
347 data). For angle-dependent reflection coefficients, the amplitudes obtained at reservoir level should  
348 be convolved with the inverse source wavelet extracted from seismic and well-log data.

349 The calculated and observed data are used in the Bayesian approach and their misfit is minimised  
350 in the form of porosity or desired parameter describing the reservoir character via the objective  
351 function. The sensitivity of the desired reservoir parameter with seismic AVA amplitudes, or

352 angle-dependent reflection coefficient, is crucial for the inversion procedure, i.e. if porosity  
353 changes, the seismic AVA data must also change.

354 In a nutshell, the results presented in this study using synthetic numerical experiments are  
355 important to everyone working with AVA data. The analysis of seismic amplitude variation with  
356 angle of incidence (AVA) is commonly used in the evaluation of reservoir character. It can be very  
357 useful to know which seismic AVA model is suitable to provide reliable results during AVA  
358 analyses and seismic-data inversion.

## 359 **5 Conclusions**

360  
361 AVA analysis and inversion in isotropic media require computation of P-wave reflection  
362 coefficients between two layers with different properties. There are several approximations to the  
363 exact Zoeppritz solution for this purpose and these are often used in practice. It may be an  
364 interesting idea to investigate the accuracy of these existing approximations within the context of  
365 seismic reservoir characterization via AVA analysis or inversion. In this study, we have  
366 investigated the accuracy of AVA approximations and their implications to the determination of  
367 reservoir porosity both in synthetic forward and inverse numerical experiments.

368 Forward modelling results show that all the approximations to the exact solution, except for Fatti's  
369 and Smith's, are in good agreement with the exact Zoeppritz solutions at smaller angles of  
370 incidence. However, they start to deviate from it as incidence angle increases from  $20^\circ$ .

371 In synthetic AVA gathers, all the approximations to the exact solution show a decrease in seismic  
372 amplitude with increasing porosity, and polarity reversals at relatively small porosity values.

373 Fatti's approximation shows the largest negative amplitude, whereas Smith's approximation  
 374 returns large positive amplitudes. They are both in disagreement with the exact Zoeppritz solution.  
 375 In AVA inversion tests using Bayesian and Monte Carlo methods, Rüger and Bortfeld  
 376 approximations show a good agreement with the exact Zoeppritz solution, while the Aki and  
 377 Richard, Hiltermann and Shuey's approximations underestimate the reservoir porosity and should  
 378 be used in AVA inversion with caution. The uncertainty for Smith's approximation is significantly  
 379 high and it cannot be used in AVA inversion for reservoir porosity.

380 The *Maximum a posteriori* solution for porosity inversion shows that porosities recovered by  
 381 Rüger and Bortfeld's approximations are in good agreement with the exact Zoeppritz solution and  
 382 recover reservoir porosities to a satisfactory level. Aki and Richard, Hiltermann and Shuey's  
 383 approximations underestimate porosity and the effect is more prominent for smaller porosities.  
 384 Fatti's and Smith's approximations completely failed to recover reservoir porosity due to their  
 385 associated high uncertainty. We hope that this study will provide the readers an insight on choosing  
 386 a suitable approximation for AVA analyses and inversion as methods in reservoir characterisation.

387 **Table 1:** Elastic properties of solid mineral, fluid and overburden used in the computation of  
 388 reflection coefficients in this work ( $GPA (Gigapascal) = 10^9 Pa = 10^9 Kg . m^{-1} . s^{-2}$ ).

Material	Bulk Modulus (GPA)	Shear Modulus (GPA)	Density (g/cm <sup>3</sup> )
Quartz matrix	37.6	44	2.65
Fluid (water/brine)	2.2	0	1

Fluid (gas)	0.02	0	0.065
Overburden (Shale)	18	7	2.35

389

390

391 **Table 2:** Uncertainty percentage of different approximations for the estimation of porosity using  
 392 a *Maximum a posteriori* solution.

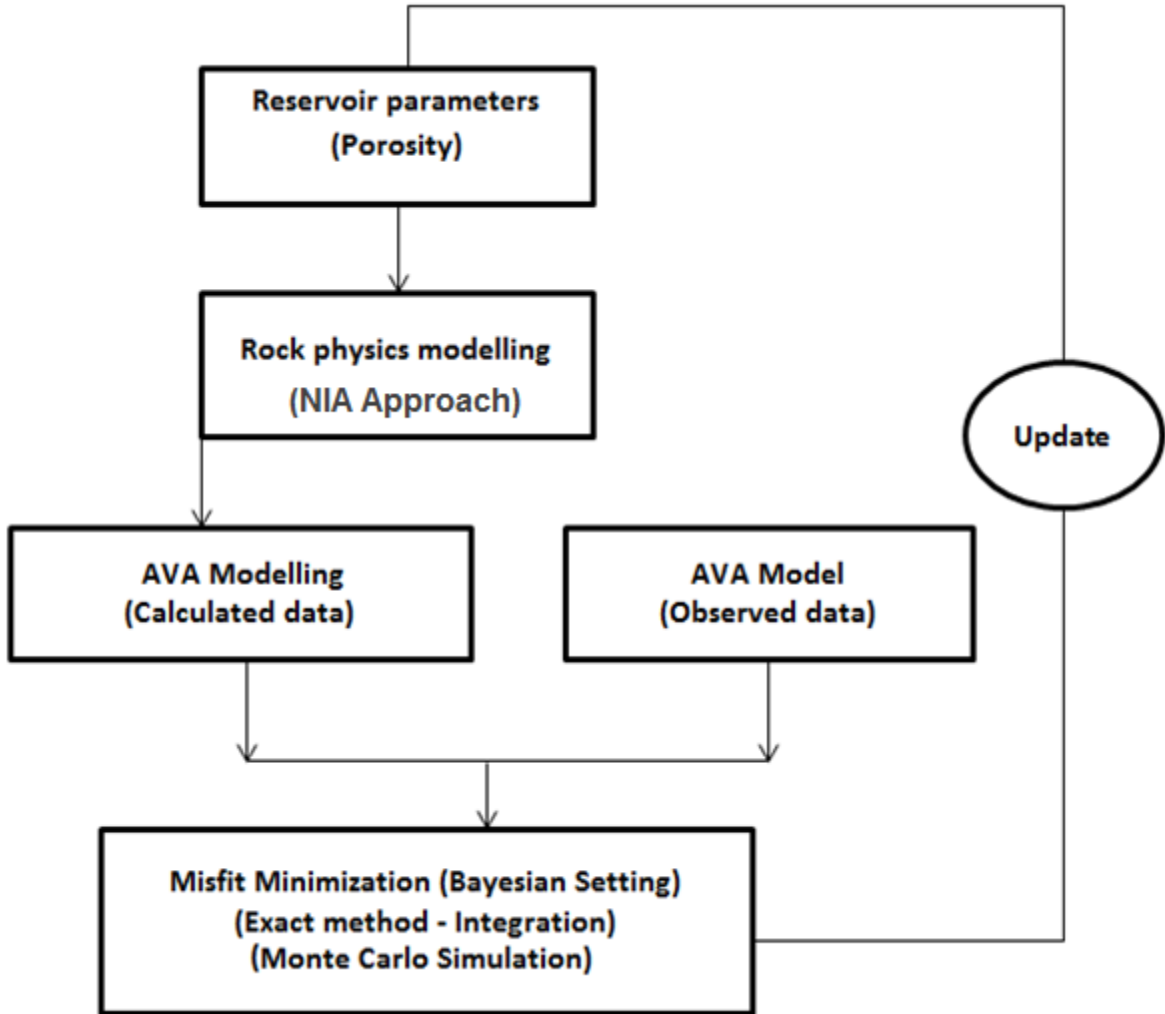
Approximation	Uncertainty (%)	Status	Remarks
Shuey	53	Underestimates porosity	Should be used with caution
Hilterman	67	Considerably underestimates porosity	Should not be used in inverse modelling
Fatti	100	Fails to recover porosity	Should not be used in inverse modelling
Aki and Richards	42	Underestimates porosity	Should be used with caution
Smith	639	High uncertainty, overestimates porosity	Should not be used in inverse modelling
Bortfeld	04	Closer to exact Zoeppritz	Satisfactory
Ruger	04	Closer to exact Zoeppritz	Satisfactory

393

394

395

396



397

398 **Figure 1:** Schematic workflow used to estimate porosity from seismic AVA analyses.

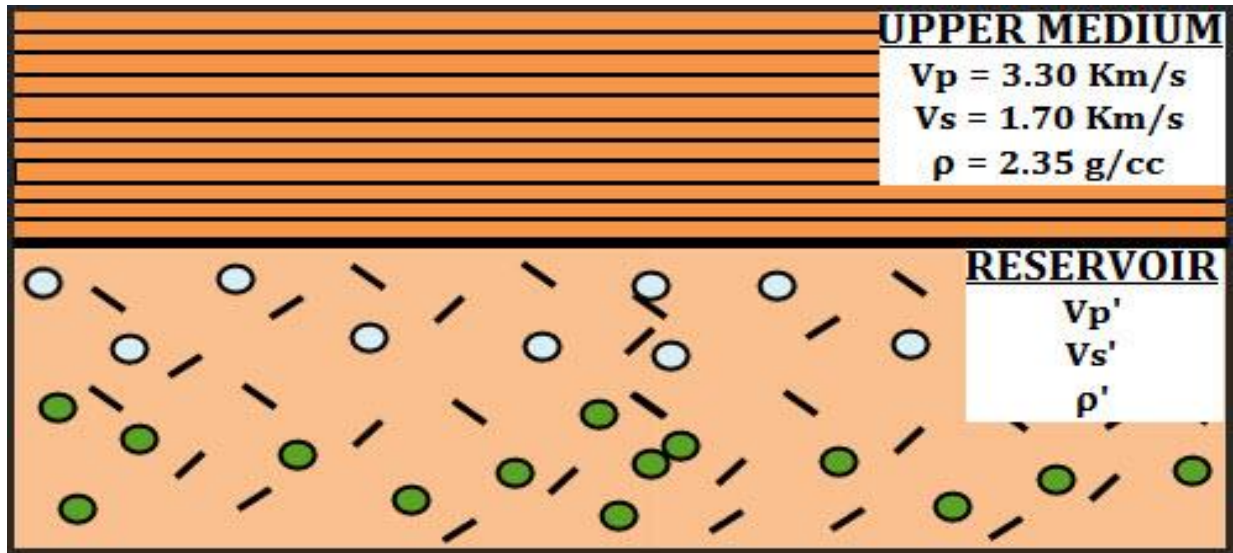
399

400

401

402

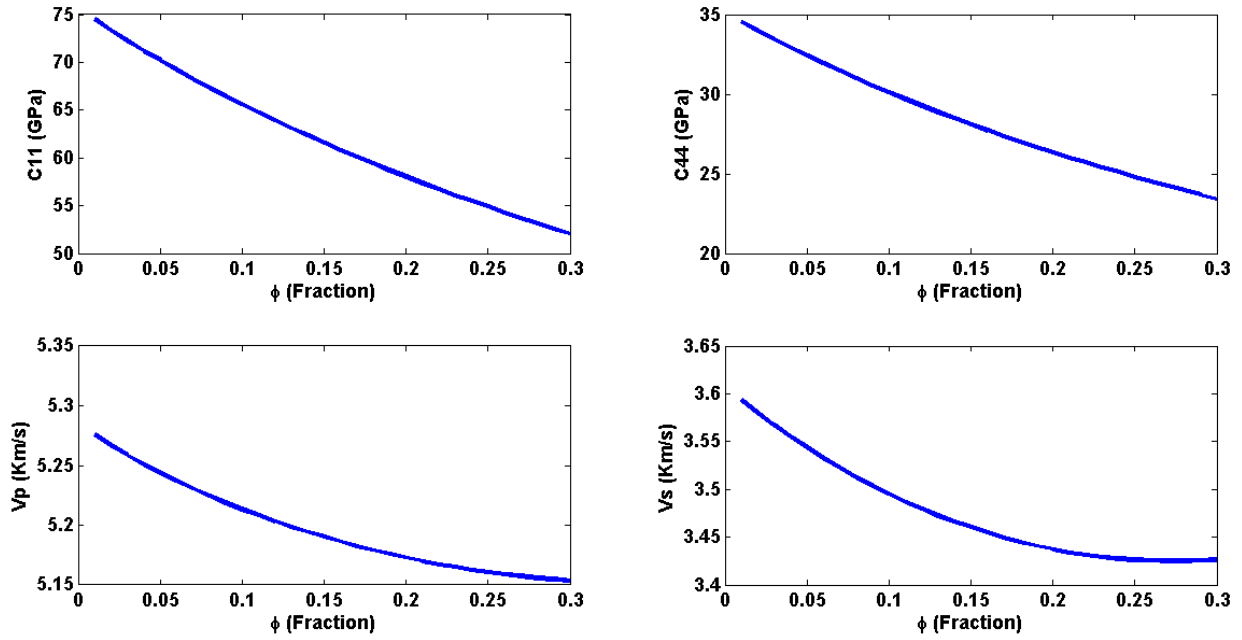
403



404

405 **Figure 2:** Rock physics model includes quartz matrix, interconnected spherical pores, and  
 406 randomly oriented micro-cracks that do not contribute to the porosity of the rock, with water and  
 407 gas as pore-saturating fluids. The aspect ratio of randomly oriented micro-cracks was set to 1/1000.

408



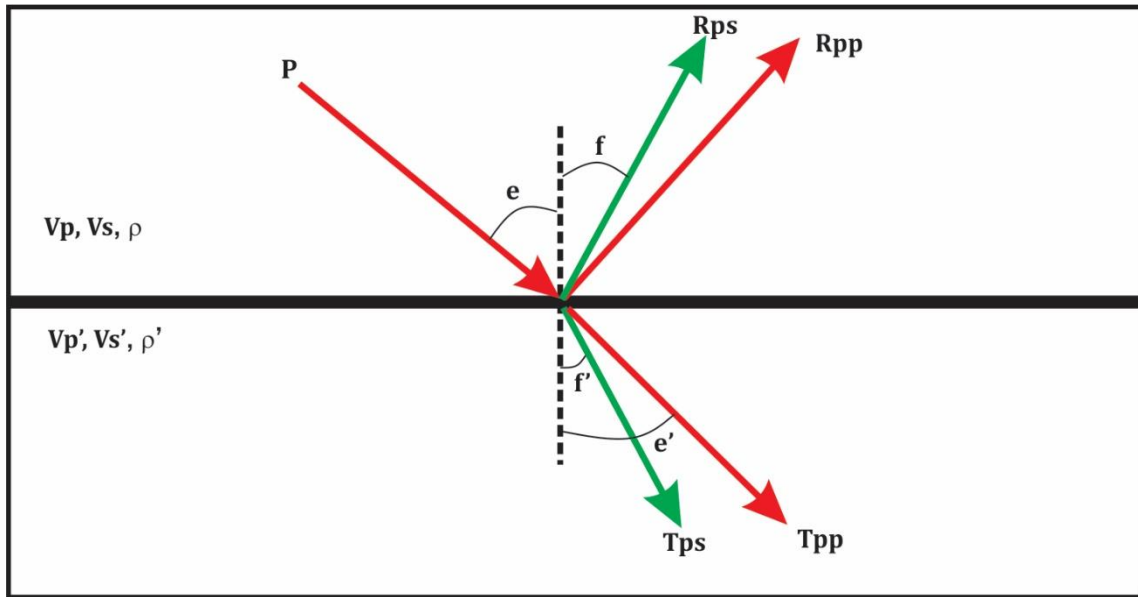
409

410 **Figure 3:** C11, C44 and Vp, Vs plotted against porosity show a relative decrease with increasing  
 411 porosity.

412

413

414

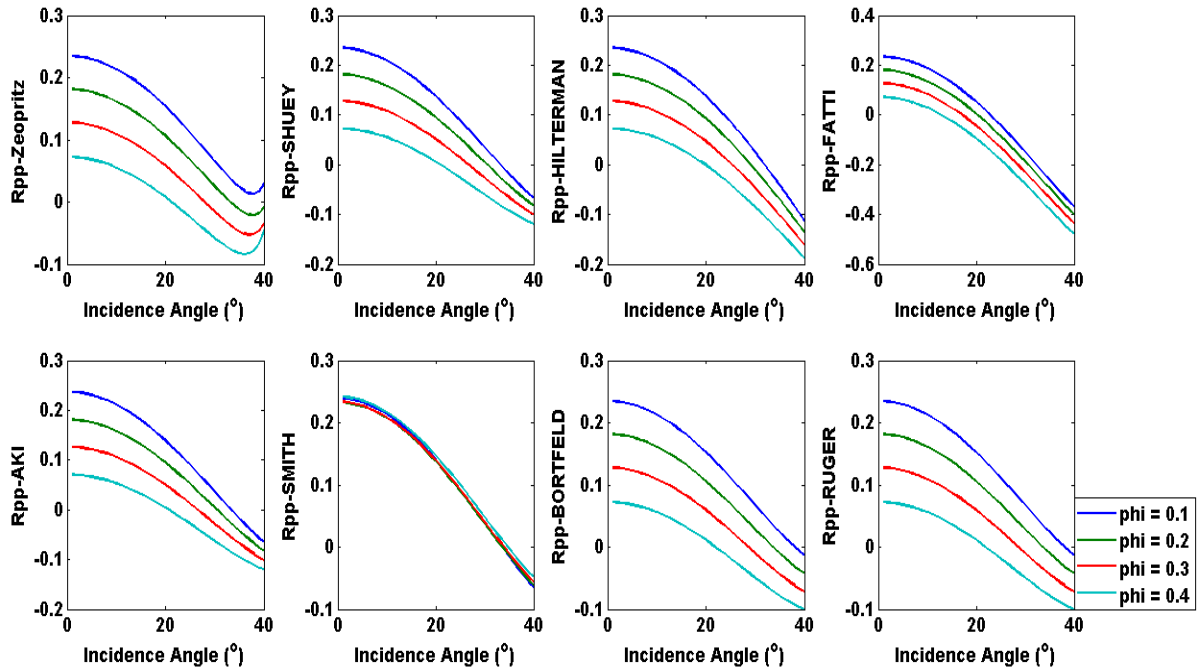


415

416 **Figure 4:** Partitioning of energy at an interface. Modified from Castagna and Backus (1993).

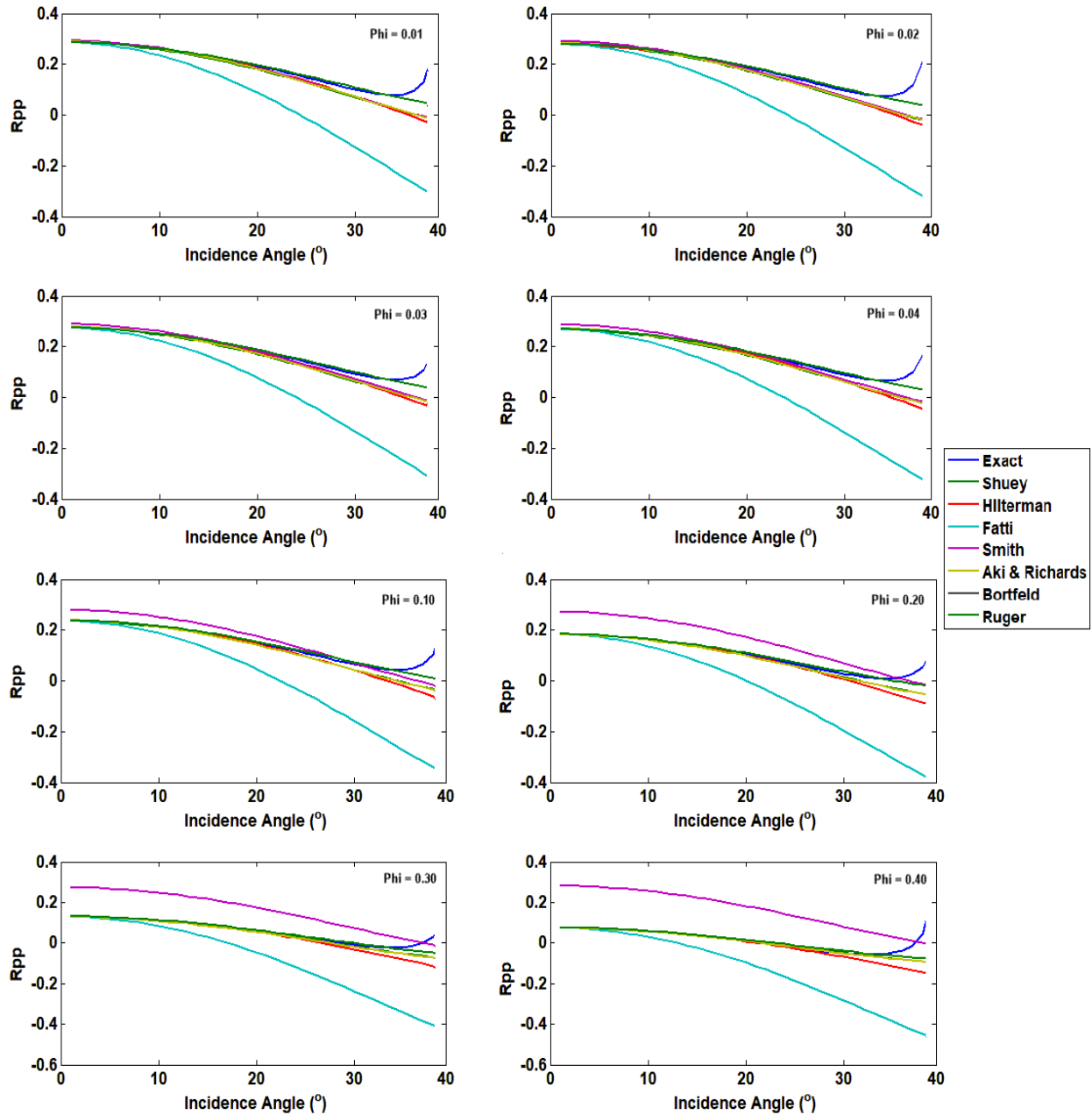
417

418



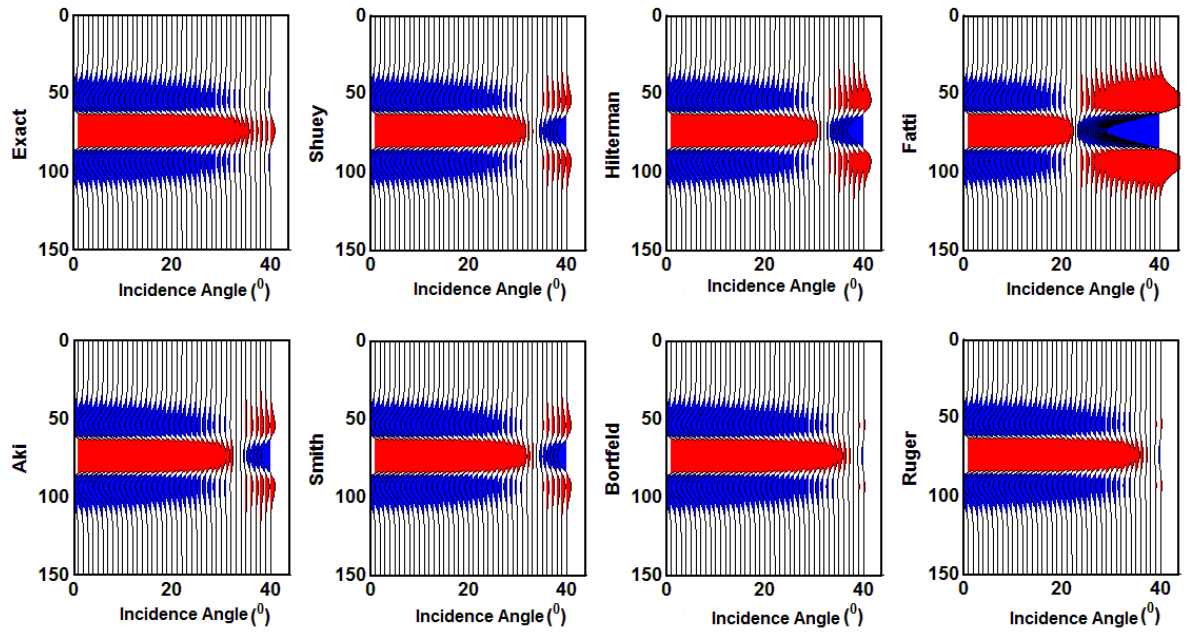
419

420 **Figure 5:** Reflection Coefficient (RC) sensitivity to porosity. The exact Zoeppritz equation, and  
 421 all its approximations show a general decrease in reflection coefficient with increasing angles of  
 422 incidence and porosity. The properties of overburden rocks are given in Table 1.



423

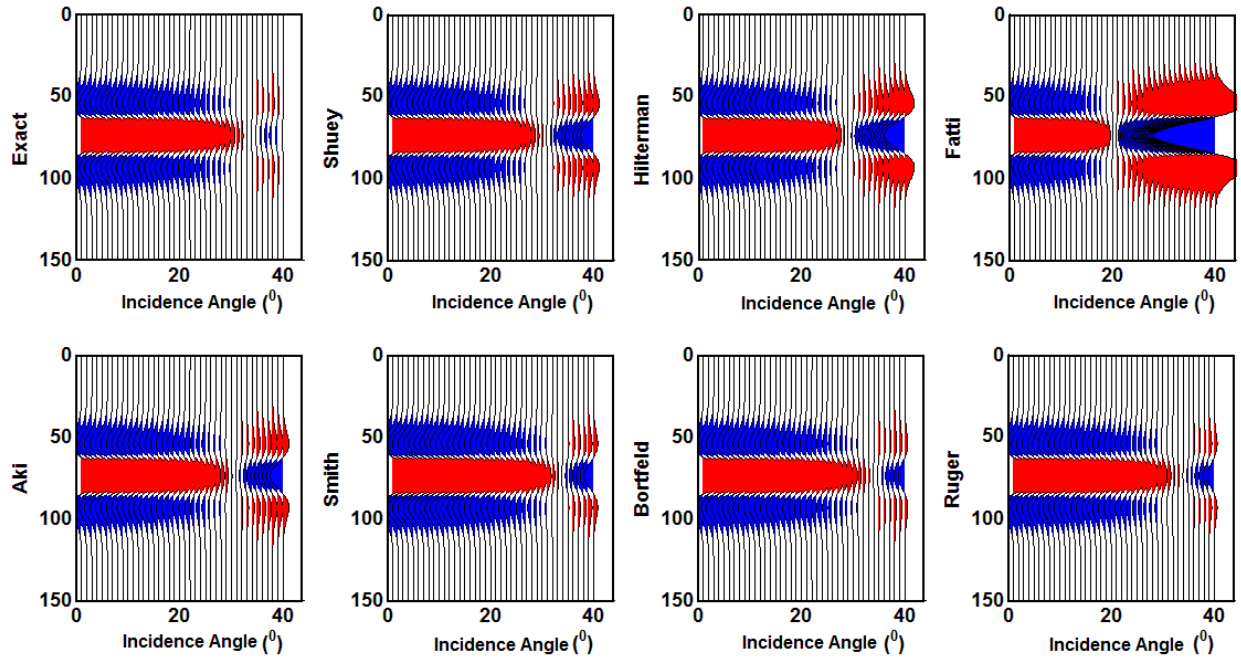
424 **Figure 6:** Comparison between the exact Zoeppritz solution, and approximations to the exact  
 425 solution, for small and high porosity values. All the approximations, except for Fatti and Smith's,  
 426 are in agreement with Zoeppritz's at small incidence angles (between  $0^\circ$  and  $20^\circ$ ), and deviate from  
 427 it at large incidence angles. The properties of overburden rocks are given in Table 1.



428

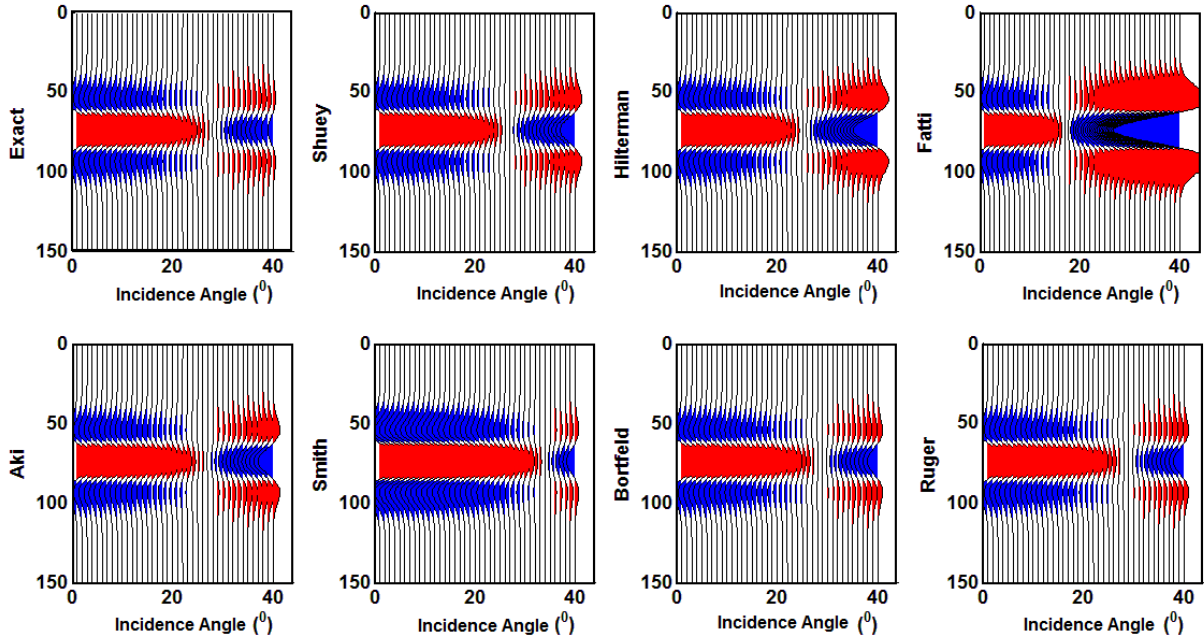
429 **Figure 7:** AVA response of the exact Zoeppritz and approximations to the exact solution (Phi-  
 430 Fraction = 0.10).

431



432

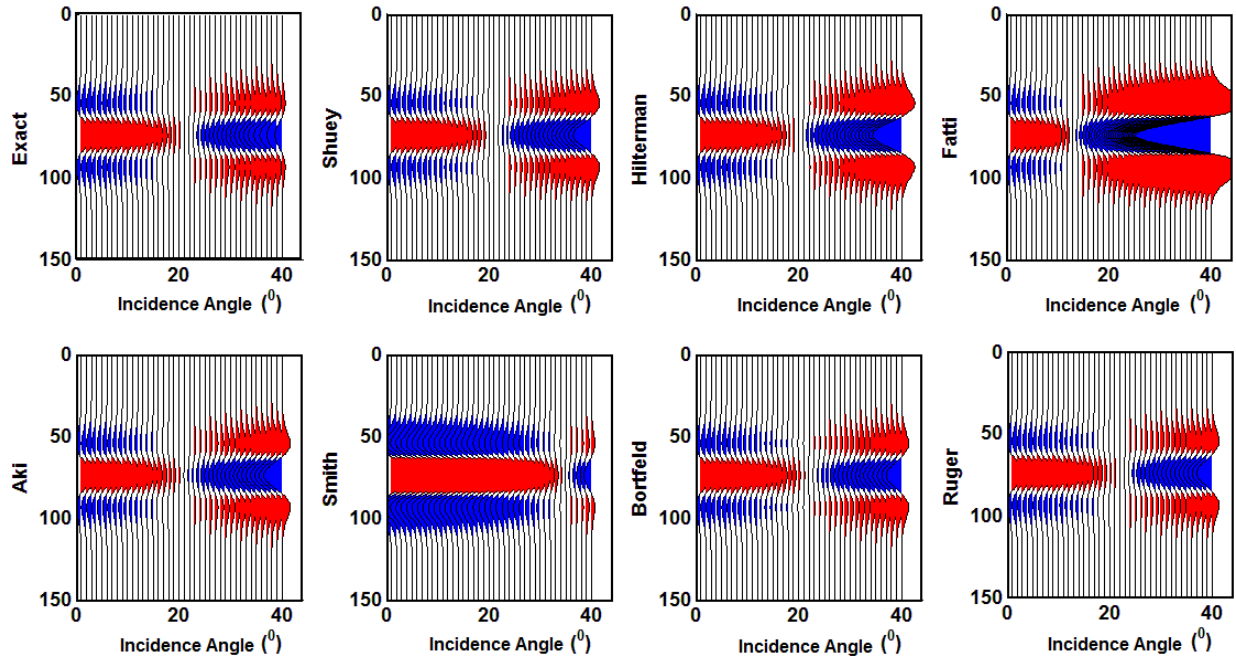
433 **Figure 8:** AVA response of the exact Zoeppritz equation and its approximations to the exact  
 434 solution ( $\Phi$ -Fraction = 0.20). Every approximation shows polarity reversal at relatively large  
 435 incident angles.



436

437 **Figure 9:** AVA response of the exact Zoeppritz equation and its approximations to the exact  
 438 solution (Phi-Fraction = 0.30).

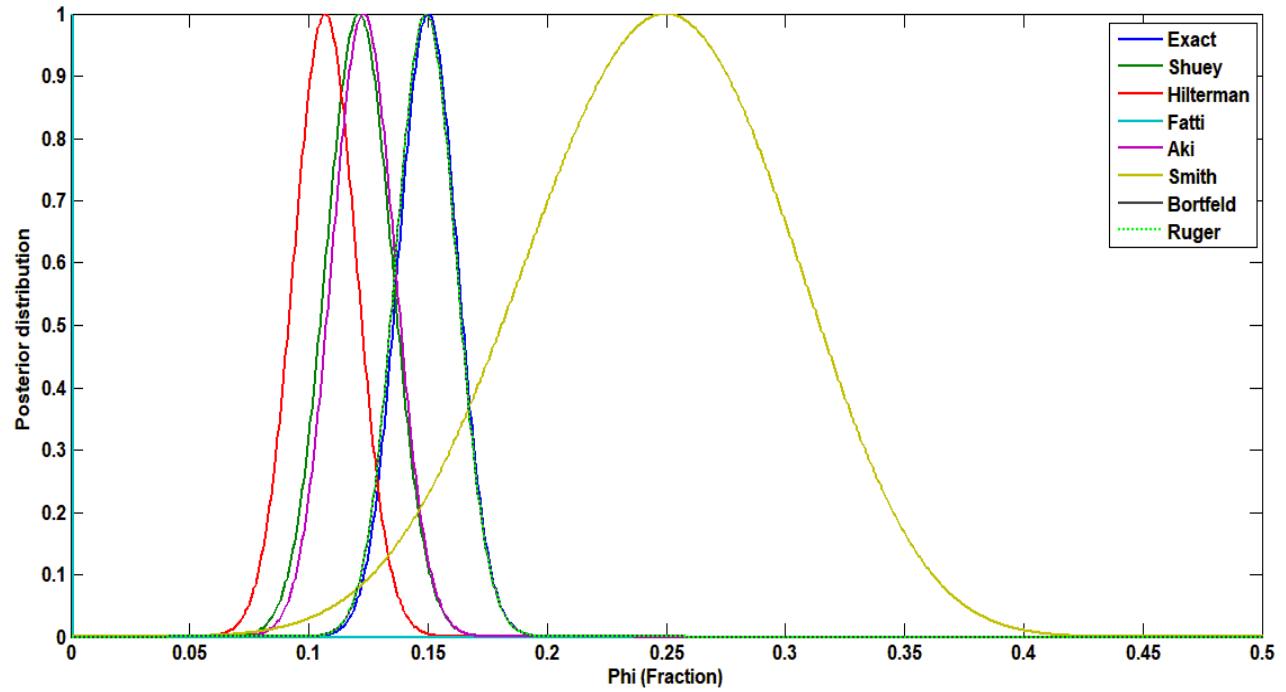
439



440

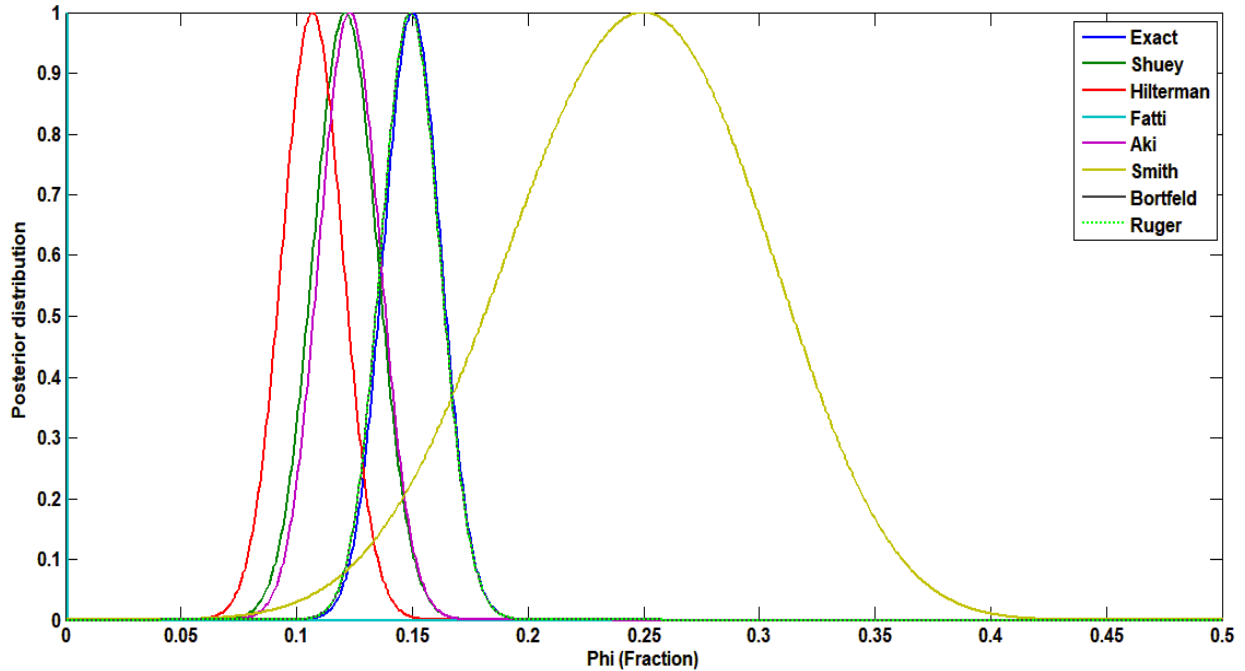
441 **Figure 10:** AVA response of the exact Zoeppritz and approximations to the exact solution (Phi-

442 Fraction = 0.40).



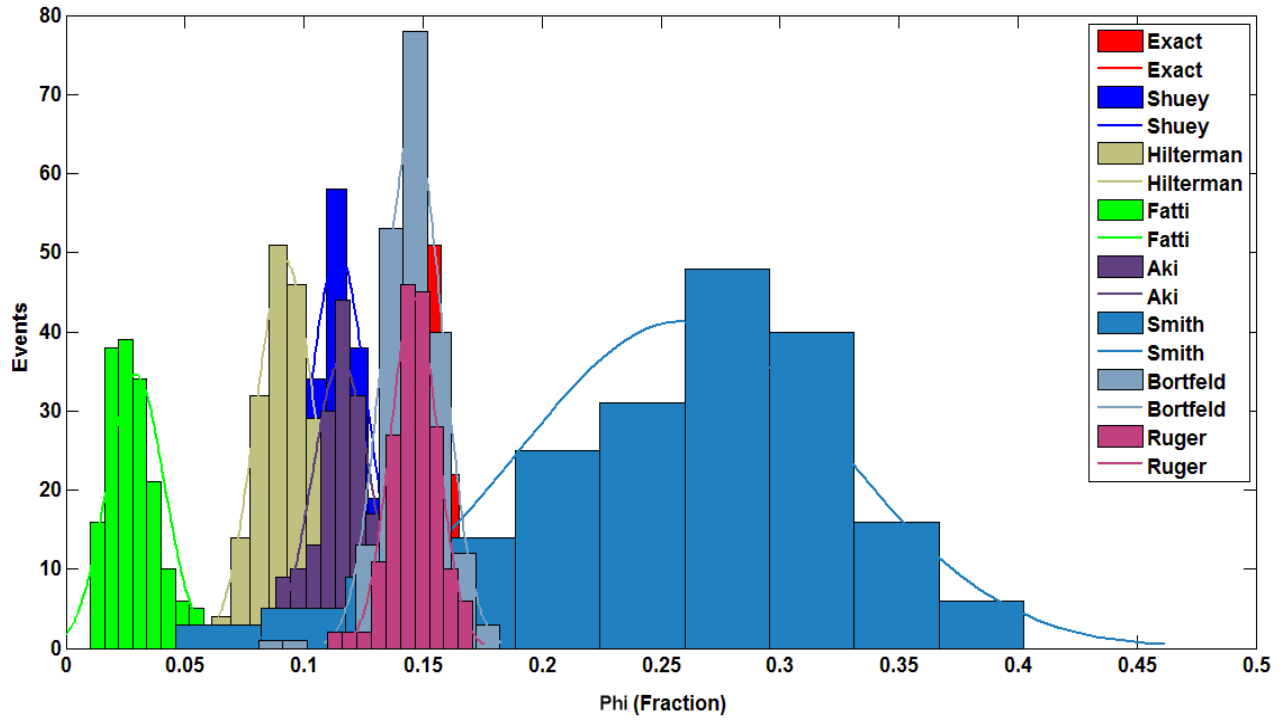
443

444 **Figure 11:** Results of the Bayesian inversion for porosity from angle-dependent reflectivity data  
 445 (for incident angle ranging between  $0^0$  and  $40^0$  degrees) using the exact Zoeppritz equations and  
 446 its approximations. True porosity is set at 0.15. The Rüger and Bortfeld approximations are in  
 447 good agreement with the Zoeppritz solution. Aki and Richards, Shuey and Hilterman's  
 448 approximations underestimate porosity. The uncertainty for Smith's approximation is very large,  
 449 and Fatti's approximation failed to recover a meaningful value for porosity.



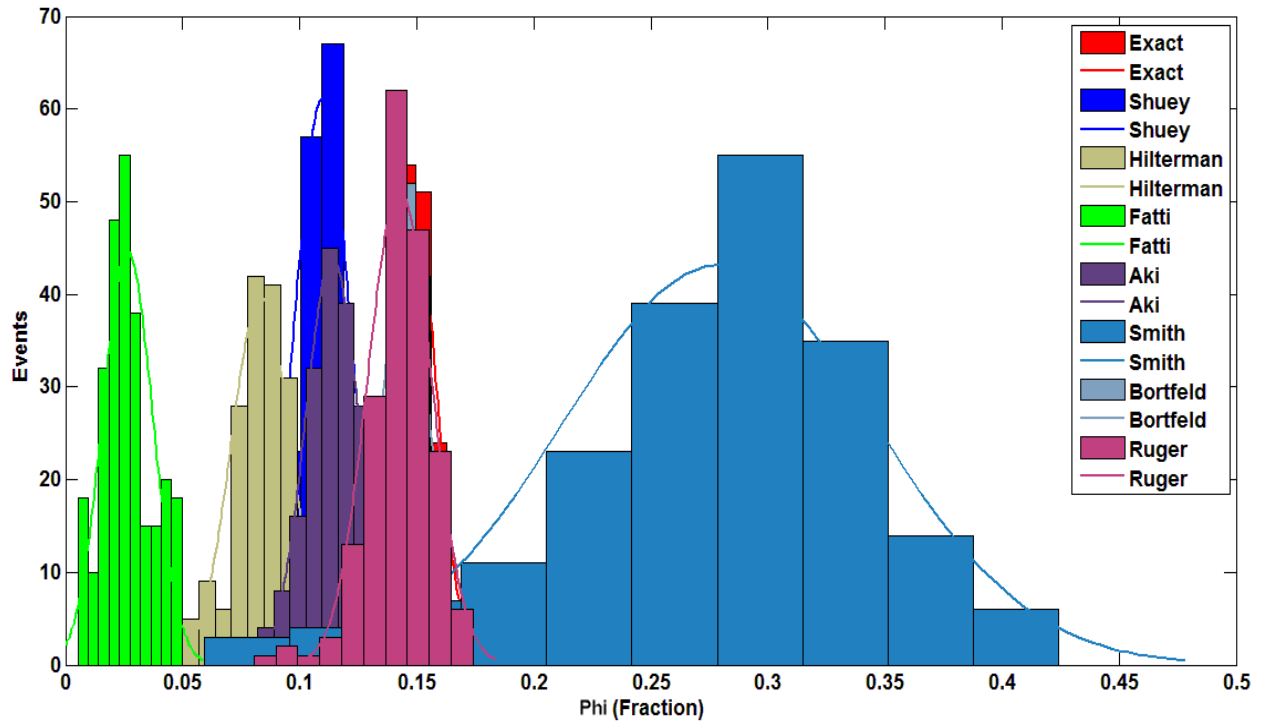
450

451 **Figure 12:** Results of the Bayesian inversion for porosity from synthetic AVA gathers (for incident  
 452 angle ranging between  $0^{\circ}$  and  $40^{\circ}$  degrees) using the exact Zoeppritz equation and its  
 453 approximations. True porosity is set at 0.15. The Rüger and Bortfeld approximations are in good  
 454 agreement with the Zoeppritz solution. Aki and Richards, Shuey and Hilterman's approximations  
 455 underestimate porosity. The uncertainty for Smith's approximation is very large and Fatti's  
 456 approximation failed to recover a meaningful value for porosity.



457

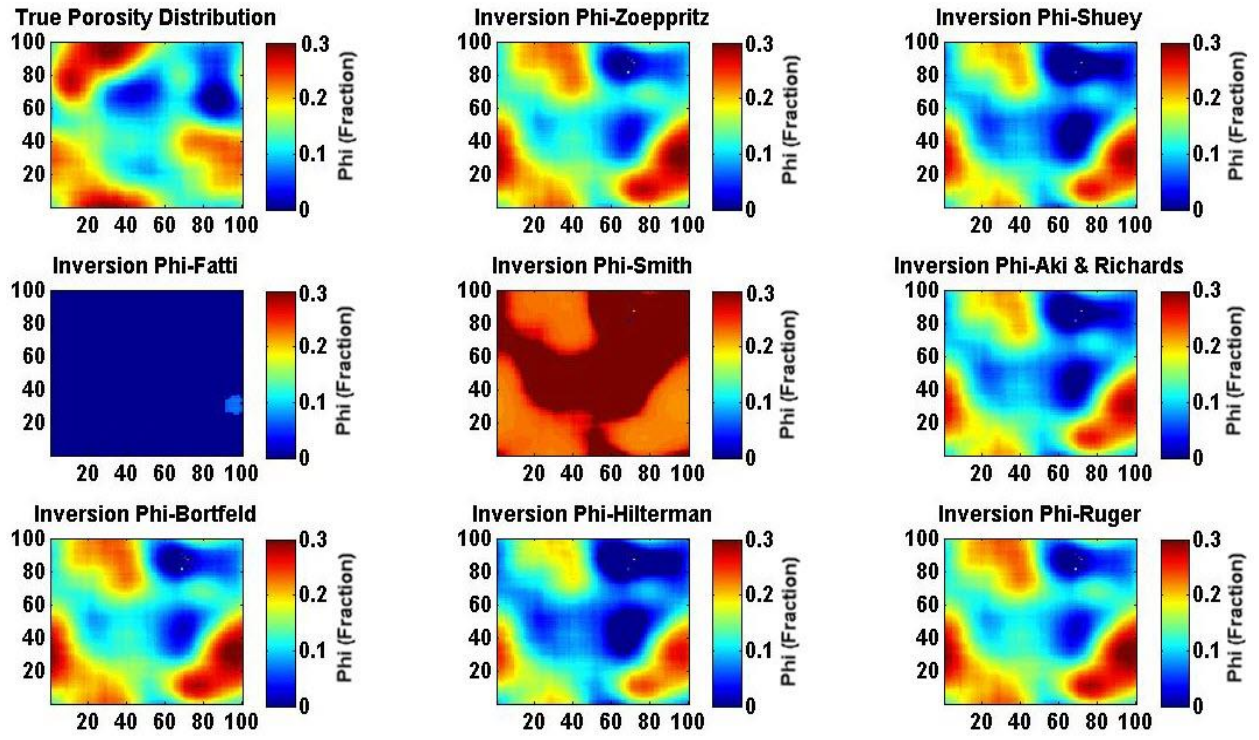
458 **Figure 13:** Monte Carlo method for sampling the *a posteriori* distribution for porosity from angle-  
 459 dependent reflectivity data (incidence angles between  $0^{\circ}$  and  $40^{\circ}$ degrees). True porosity is set to  
 460 0.15.



461

462 **Figure 14:** Monte Carlo method for sampling the *a posteriori* distribution for porosity from  
 463 synthetic AVA gathers (incidence angles between  $0^0$  and  $40^0$  degrees). True porosity is set to 0.15.

464



465

466 **Figure 15:** *Maximum a posteriori* solution used to recover the reservoir porosity distribution, for  
 467 the exact Zoeppritz equation and its approximations under 25% noise settings. Aki and Richards,  
 468 Bortfeld, Shuey and R uger's approximations recover reservoir porosity distribution up to some  
 469 extent, but Fatti and Smith's approximations failed to recover porosity to a satisfactory level.

470

471

472

## References

- 473
- 474 Aki, K., and Richards, P. G. (1980). Quantitative Seismology: Theory and Methods. Freeman and  
475 Co.
- 476 Ali, A., Anwer, H.M., and Hussain, M. (2015). A comparisomal study in the context of seismic  
477 fracture characterization based on effective stiffness and compliance methods. *Arabian Journal of*  
478 *Geosciences*, 8(6), 4117-4125.
- 479 Ali, A., and Jakobsen, M. (2011a). On the accuracy of Rüger's approximation for reflection  
480 coefficients in HTI media: implications for the determination of fracture density and orientation  
481 from seismic AVAZ data. *Journal of Geophysics and Engineering*, 8(2), 372.
- 482 Ali, A., and Jakobsen, M., (2011b). Seismic characterization of reservoirs with multiple fracture  
483 sets using velocity and attenuation anisotropy data. *Journal of Applied Geophysics*, 75:590–602
- 484 Ali, A., and Jakobsen, M. (2014). Anisotropic permeability in fractured reservoirs from frequency-  
485 dependent seismic Amplitude Versus Angle and Azimuth data. *Geophysical Prospecting*, 62(2),  
486 293-314.
- 487 Anwer, H. M., Ali, A., and Alves, T.M. (2017). Bayesian inversion of synthetic AVO data to assess  
488 fluid and shale content in sand-shale media. *Journal of Earth System Science*, 126(3), 42.
- 489 Aster, R.C., Borchers, B., and Thurber, C. H. (2005). Parameter Estimation and Inverse Problems.  
490 Academic Press.
- 491 Avseth, P., Mukerji, T., and Mavko, G. (2005). Quantitative seismic interpretation: Applying rock  
492 physics tools to reduce interpretation risk. Cambridge University Press

493 Bortfeld, R. (1961). Approximations to the reflection and transmission coefficients of plane  
494 longitudinal and transverse waves. *Geophysical Prospecting*, 9(4), 485-502.

495 Bosch, M., Mukerji, T., and Gonzalez, E. F. (2010). Seismic inversion for reservoir properties  
496 combining statistical rock physics and geostatistics: A review. *Geophysics*, 75(5), 75A165-  
497 75A176.

498 Buland, A., Omre, H., (2003). Bayesian linearized AVO inversion. *Geophysics*, 68, 185-198.

499 Castagna, J. P., and Backus, M. M. (1993). AVO analysis—Tutorial and review. Offset-dependent  
500 reflectivity. *Theory and practice of AVO analysis: SEG Investigations in Geophysics*, (8), 3-36.

501 Castagna, J. P., and Swan, H. W. (1997). Principles of AVO cross-plotting. *The leading*  
502 *Edge*, 16(4), 337-344.

503 Chiappa, F., and Mazzotti, A. (2009). Estimation of petrophysical parameters by linearized  
504 inversion of angle domain pre-stack data. *Geophysical Prospecting*, 57(3), 413-426.

505 Chiburis, E.F., 1984, Analysis of amplitude versus offset to detect gas-oil contacts in Arabia Gulf:  
506 54th Ann. Internat. Mtg., Soc. Expl. Geophys., Expanded Abstracts, 669-670.

507 Du, Q., and Yan, H. (2013). PP and PS joint AVO inversion and fluid prediction. *Journal of*  
508 *Applied Geophysics*, 90, 110-118.

509 Duijndam, A. J. W. (1988a). Bayesian Estimation in Seismic Inversion. Part-I:  
510 Principles. *Geophysical Prospecting*, 36(8), 878-898.

511 Duijndam, A. J. W. (1988b). Bayesian Estimation in Seismic Inversion. Part II: Uncertainty  
512 Analysis. *Geophysical Prospecting*, 36(8), 899-918.

513 Eshelby, J. D. (1957, August). The determination of the elastic field of an ellipsoidal inclusion,  
514 and related problems. In: *Proceedings of the Royal Society of London A: Mathematical, Physical*  
515 *and Engineering Sciences* (Vol. 241, No. 1226, pp. 376-396).

516 Fatti, J. L., Smith, G. C., Vail, P. J., Strauss, P. J., and Levitt, P. R. (1994). Detection of gas in  
517 sandstone reservoirs using AVO analysis: A 3-D seismic case history using the Geo stack  
518 technique. *Geophysics*, 59(9), 1362-1376.

519 Gassmann, F. (1951). Über die elastizität poröser medien: Vierteljahrsschrift der  
520 Naturforschenden Gesellschaft in Zurich 96, 1-23. *Paper translation at <http://sepwww.stanford.edu/sep/berryman/PS/gassmann.pdf>*.

522 Green, G. (1839). On the law of reflection and refraction of light. *Transactions of the Cambridge*  
523 *Philosophical Society*, 7.

524 Grossman, J.P. (2003). AVO and AVA inversion challenges: a conceptual overview. Crewes  
525 Research Report, 15.

526 Hastings, W.K. (1970). Monte Carlo sampling methods using Markov chains and their  
527 applications. *Biometrika*, 57(1), 97-109.

528 Hilterman, F.J. (1989). Is AVO the seismic signature of rock properties? In 1989 SEG Annual  
529 Meeting. Society of Exploration Geophysicists.

530 Houck, R.T. (2002). Quantifying the uncertainty in an AVO interpretation. *Geophysics*, 67(1),  
531 117-125.

532 Hudson, J.A., and Knopoff, L. (1989). Predicting the overall properties of composite materials  
533 with small-scale inclusions or cracks. *Pure and Applied Geophysics*, 131(4), 551-576.

534 Hu, Y., and McMechan, G.A. (2009): Comparison of effective stiffness and compliance for  
535 characterising cracked rocks, *Geophysics*, 74, D49-D55.

536 Jakobsen, M., and Johansen, T.A. (2005). The effects of drained and undrained loading on visco-  
537 elastic waves in rock-like composites. *International Journal of Solids and Structures*, 42(5), 1597-  
538 1611.

539 Jakobsen, M., Hudson, J.A., and Johansen, T.A. (2003). T-matrix approach to shale  
540 acoustics. *Geophysical Journal International*, 154(2), 533-558.

541 Knott, C.G. (1899). Reflection and refraction of elastic waves, with seismological  
542 applications. *The London, Edinburgh, and Dublin Philosophical Magazine and Journal of*  
543 *Science*, 48(290), 64-97.

544 Krebes, E.S. (2004). Seismic forward modelling. *CSEG Recorder*, 30, 28-39.

545 Liang, L., Zhang, H., Guo, Q., Saeed, W., Shang, Z., and Huang, G. (2017). Stability study of pre-  
546 stack seismic inversion based on the full Zoeppritz equation. *Journal of Geophysics and*  
547 *Engineering*, 14(5), 1242.

548 Marfurt K.J., and Alves, T.M. (2015). Pitfalls and limitations in seismic attribute interpretation  
549 of tectonic features. *Interpretation*, 3(1), SB5-SB15. doi: 10.1190/INT-2014-0122.1

550 Metropolis, N., and Ulam, S. (1949). The Monte Carlo method. *Journal of the American Statistical*  
551 *Association*, 44(247), 335-341.

552 Metropolis, N., Rosenbluth, A.W., Rosenbluth, M.N., Teller, A.H., and Teller, E. (1953). Equation  
553 of state calculations by fast computing machines. *The Journal of Chemical Physics*, 21(6), 1087-  
554 1092.

555 Mukerji, T., Avseth, P., Mavko, G., Takahashi, I., and González, E.F. (2001). Statistical rock  
556 physics: Combining rock physics, information theory, and geostatistics to reduce uncertainty in  
557 seismic reservoir characterization. *The Leading Edge*, 20(3), 313-319.

558 Ostrander, W.J., 1984, Plane-wave reflection coefficients for gas sands at nonnormal angles of  
559 incidence. *Geophysics*, 49, 1637-1648.

560 Pujol, J. (2003). Elastic wave propagation and generation in seismology. Cambridge University  
561 Press.

562 Ren, H., Ray, J., Hou, Z., Huang, M., Bao, J., and Swiler, L. (2017). Bayesian inversion of seismic  
563 and electromagnetic data for marine gas reservoir characterization using multi-chain Markov chain  
564 Monte Carlo sampling. *Journal of Applied Geophysics*, 147, 68-80.

565 Rüger, A., 2002. Reflection Coefficients and Azimuthal AVO Analysis in Anisotropic Media.  
566 *Geophysical Monograph Series*, Number 10, Soc. of Expl. Geophys.

567 Rutherford, S.R., and Williams, R.H. (1989). Amplitude-versus-offset variations in gas  
568 sands. *Geophysics*, 54(6), 680-688.

569 Shahraini, A., Ali, A., and Jakobsen, M. (2011). Characterization of fractured reservoirs using a  
570 consistent stiffness-permeability model: focus on the effects of fracture aperture. *Geophysical*  
571 *Prospecting*, 59(3), 492-505.

572 Shuey, R. T. (1985). A simplification of the Zoeppritz equations. *Geophysics*, 50(4), 609-614.

573 Smith, G.C., and Gidlow, P.M. (1987). Weighted stacking for rock property estimation and  
574 detection of GAS. *Geophysical Prospecting*, 35(9), 993-1014.

575 Sun, S. Z., Yang, P., Liu, L., Sun, X., Liu, Z., and Zhang, Y. (2015). Ultimate use of prestack  
576 seismic data: Integration of rock physics, amplitude-preserved processing, and elastic  
577 inversion. *The Leading Edge*, 34(3), 308-314.

578 Tarantola, A. (2005). Inverse problem theory and methods for model parameter estimation. SIAM.  
579 ISBN 0898715725.

580 Thomsen, L. (1986). Weak elastic anisotropy. *Geophysics*, 51(10), 1954-1966.

581 Thomsen, L. (1995). Elastic anisotropy due to aligned cracks in porous rock. *Geophysical*  
582 *Prospecting*, 43(6), 805-829.

583 Wang, Z. (2001). Fundamentals of seismic rock physics. *Geophysics*, 66(2), 398-412.

584 Wood, A.B. (1955). A textbook of sound. The MacMillan Co.

585 Zhang, Y., Ratcliffe, A., Roberts, G., and Duan, L. (2014). Amplitude-preserving reverse time  
586 migration: From reflectivity to velocity and impedance inversion. *Geophysics*, 79(6), S271-S283.

587 Zoeppritz, K. (1919). Erdbebenwellen VIII B. On the reflection and propagation of seismic  
588 waves. *Göttinger Nachrichten*, 1(5), 66-84.